Detection of fibril nucleation in micrometer-sized protein condensates and suppression of Sup35NM fibril nucleation by liquid-liquid phase separation

Mao Fukuyama[a,b,*], Suguru Nishinami[c], Yoko Maruyama[a], Taiki Ozawa[a], Shunsuke Tomita[d], Yumiko Ohhashi[e], Motohiro Kasuya[f], Masao Gen[a], Eri Chatani[e], Kentaro Shiraki[c], and Akihide Hibara[a,g,*]

[a]Institute of Multidisciplinary Research for Advanced Materials, Tohoku University, 2-1-1, Katahira, Sendai, Miyagi 980-8577, Japan

[b]Organization for Advanced Studies, Tohoku University, 2-1-1 Katahira, Sendai, Miyagi 980-8577, Japan

[c]Faculty of Pure and Applied Sciences, University of Tsukuba,1-1-1, Tennoudai, Tsukuba, Ibaraki 305-8573, Japan

[d]Health and Medical Research Institute, The National Institute of Advanced Industrial Science and Technology, 1-1-1 Higashi, Tsukuba, Ibaraki 305-8566, Japan

[e]Graduate School of Science Kobe University, 1-1, Rokkoudaichou, Nada, Kobe, Hyogo 657-8501, Japan

[f]Faculty of Production Systems Engineering and Sciences Komatsu University, Nu 1-3, Yonchoumemachi, Komatsu, Ishikawa 923-0971, Japan

[g]Riken, 2-1, Hirosawa, Wako, Saitama 351-0198, Japan

Corresponding Author

Mao Fukuyama and Akihide Hibara. 2-1-1 Katahira, Aokbaku, Sendai, Miyagi, 980-8577, Japan. +81-22-217-5396

Email: maofukuyama@tohoku.ac.jp,

Akihide Hibara: 2-1-1 Katahira, Aokbaku, Sendai, Miyagi, 980-8577, Japan. +81-22-217-5396

Email: hibara@tohoku.ac.jp

Abstract: Elucidating the link between amyloid fibril formation and liquid–liquid phase separation (LLPS) is crucial in understanding the pathologies of various intractable human diseases. However, the effect of condensed protein droplets generated by LLPS on nucleation (the initial step of amyloid formation) remains unclear because of the lack of available quantitative analysis techniques. This study aimed to develop a measurement method for the amyloid droplet nucleation rate based on image analysis. We developed a method to fix micrometer-sized droplets in gel for long-term observation of protein droplets with known droplet volumes. By combining this method with image analysis, we determined the nucleation dynamics in droplets of a prion disease model protein, Sup35NM, at the single-event level. We found that the nucleation was unexpectedly suppressed by LLPS above the critical concentration (C*) and enhanced below C*. We also revealed that the lag time in the Thioflavin T assay, a semi-quantitative parameter of amyloid nucleation rate, does not necessarily reflect nucleation tendencies in droplets. Our results suggest that LLPS can suppress amyloid nucleation, contrary to the conventional hypothesis that LLPS enhances it. We believe that the proposed quantitative analytical method will provide insights into the role of LLPS from a pathological perspective.

Introduction

Formation of protein aggregates, including amyloid fibrils, is a ubiquitous process in nature and is often associated with

human diseases, such as amyotrophic lateral sclerosis, Huntington's disease, and Parkinson's disease[1,2]. Typically, these fibrils form an ordered cross-β structure, in which β-strands are stacked perpendicular to the longer axis of each fibril. The formation of amyloid aggregates is described by the nucleation-dependent model, a process that comprises nucleation and elongation of fibrils, which is the same as protein crystallization[3,4]. In this model, nucleation is rare and reversible, and fibril elongation irreversibly proceeds once nucleation occurs. The nucleation of amyloid fibrils has been widely investigated because it is a critical process in amyloid generation[5,6].

Many amyloidogenic proteins, including α-synuclein[7], FUS[8], Tau[9,10], TDP-43[11], TIA-1[12], hnRNPA1[13], and Sup35[14], undergo liquid-liquid phase separation (LLPS) in cells, forming small, liquid-like droplets (Figure 1A). During biological LLPS of proteins, a protein-condensed phase (in the form of droplets, $C_{droplet}$) spontaneously appears in the protein-depleted phase (C'), whereas the protein amount (M) is preserved. Intrinsically disordered regions (IDRs), which are commonly contained in amyloidogenic proteins, induce LLPS through weak multivalent intermolecular interactions, such as electrostatic, cation-π, and π-π interactions[15–17].

Because the protein concentration in the droplets formed by LLPS is extremely high (typically 200–300 mg/mL)[18], droplet formation of amyloidogenic proteins is thought to increase the risk of amyloid generation by promoting aggregation in cells[7]. Amyloid generation in droplets has been often observed both *in vitro*[8,11–13,19–21] and *in silico*[22]. Simulations predict that the nucleation barrier decreases or becomes negligible (as in spinodal decomposition) in such a high concentration range, according to several nucleation theories[22–25]. However, it is usually impossible to quantify amyloid nucleation within droplets because of the irreversibility of droplet coalescence and size growth during the observation process. Thus, our knowledge of amyloid nucleation kinetics in droplets is still limited because of the lack of existing quantitative droplet-focused measurement methods. As physicochemical properties and molecular interactions in droplets are largely different from those in aqueous solutions[26], it is difficult to predict the amyloid nucleation kinetics in droplets by extrapolating that in aqueous solutions.

Here, we propose a quantitative analysis method for amyloid nucleation in droplets based on image analysis to reveal the nucleation kinetics. We developed a method to fix micrometer-sized droplets in a gel to examine the kinetics of amyloid nucleation within droplets. This method allows for long-term observation of protein droplets with known droplet volumes. The nucleation rate was calculated by counting the droplets where nucleation occurred in the micrographs. We chose the Sup35 NM domain (Sup35NM) as a model protein of prion diseases[27–31] and compared the nucleation kinetics between the droplet and aqueous solution. We found the critical concentration (C*) of Sup35NM (Figure 1B); amyloid nucleation was suppressed by LLPS above C* but was enhanced below C*. This finding provides insights into the effect of LLPS on amyloid formation *in vivo*.

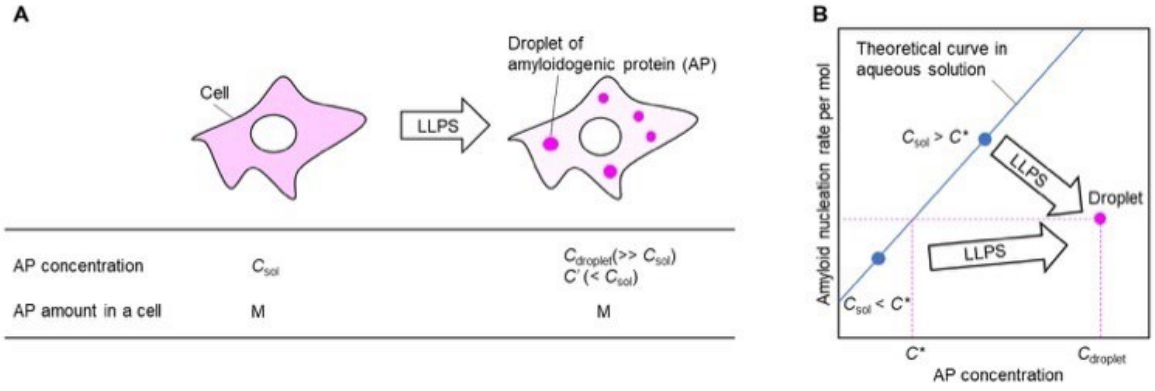

Figure 1. Effect of liquid–liquid phase separation on amyloid nucleation. (A) Schematic images of the amounts and concentrations of amyloidogenic protein (AP) before and after LLPS. AP concentration increases inside droplets ($C_{droplet} >> C_{sol}$) and decreases outside droplets (protein-depleted phase $C' < C_{sol}$), whereas the AP amount in a cell (M) is preserved. (B) A schematic illustration describing the effect of AP concentration on amyloid nucleation rate. Amyloid nucleation is suppressed by LLPS when $C_{sol} > C^*$, whereas it is enhanced when $C_{sol} < C^*$. Details are discussed in Figure 4.

Results

For long-term observation of amyloid generation from Sup35NM droplets, we fixed Sup35NM droplets in agarose gel (Figure 2A)[32]. The N-terminal domain of Sup35 is a non-charged IDR relating to amyloid formation[2833], and the middle (M) domain is a charged IDR that induces pH-dependent droplet formation[14]. Sup35NM was mixed with polyethylene glycol (PEG) at pH 6 to induce LLPS[14] gelated with agarose. Spherical assemblies were observed immediately after mixing (Figure 2B). No assemblies were observed in the absence of Sup35NM or PEG (Figure S1). Rhodamine 6G (R6G), a fluorescent dye that typically accumulates in droplets[34], and thioflavin T (ThT), an amyloid indicator, were detected in the spherical assemblies. Analysis of the fluorescence intensities (FIs) of the droplets containing Alpha Fluor 488-conjugated Sup35NM (AF488Sup35NM) indicated that the concentration of AF488Sup35NM inside and outside of the assemblies was 1160 ± 150 μM and 18.2 ± 0.3 μM, respectively. The fluidity of Sup35NM in the assemblies was evaluated by fluorescence recovery after photobleaching (FRAP, Figure 2C). The recovery time of fluorescence in AF288Sup35NM assemblies (~11 s) was similar to the reported value for liquid-like Sup35 droplets (~10 s)[14], regardless of agarose addition. This behavior indicated that these assemblies were not gel-like aggregates but liquid-like droplets. Moreover, the FRAP recovery curves were consistent between assemblies and Sup35NM droplets, suggesting that agarose did not affect the motility of Sup35NM droplets.

To investigate the transfer of Sup35NM molecules between droplets, a whole AF488Sup35 droplet was bleached, and its fluorescence recovery was monitored (Droplet 1 in Figure 2D). Fluorescence did not recover for over 1 h, indicating slow molecular exchange between the droplet and solution. The FI of Droplet 2, which was close to that of Droplet 1 (Figure 2D), did not decrease after bleaching Droplet 1, showing limited Sup35NM transfer between droplets.

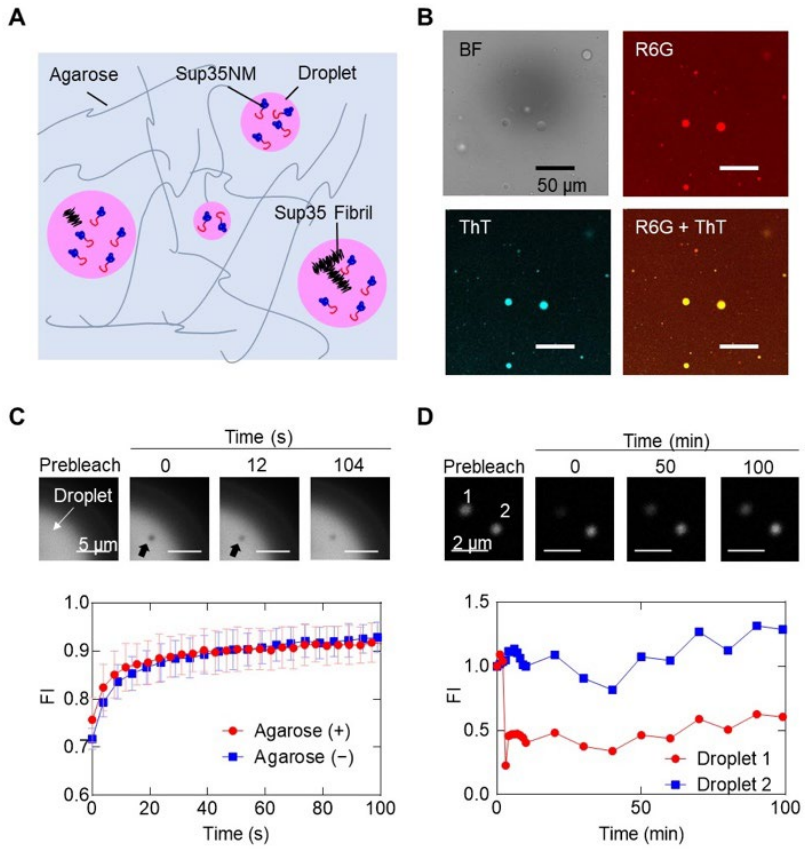

Figure 2. Sup35NM droplets in agarose gel. (A) Schematic illustration of the Sup35NM droplets fixed in agarose gel. Amyloid nucleation in these droplets was investigated. (B) Bright field and fluorescence micrographs. Fluorescence is derived from 20 μM ThT or 5 μM R6G; scale bar, 50 μm. (C) Fluorescence images of AF488Sup35NM droplets during fluorescence recovery after photobleaching (FRAP), with recovery curves. FI indicates the fluorescence intensity of the region of interest (black arrow); scale bar, 5 μm (D) Fluorescence micrographs of AF488Sup35NM droplets during whole FRAP, with recovery curves; scale bar, 2 μm.

Next, we investigated the amyloid formation rates of Sup35NM droplets dispersed in agarose gel using confocal microscopy (Figure 3A). The diameters of the observed droplets were approximately 1–20 μm. The droplets were stable, and the droplet size remained constant for 5.5 h (coefficient of variation, CV = 6%, Figure S2). We calculated the normalized FI of ThT (F, Equation S1 in Supporting Information), which is proportional to ThT concentration, to evaluate amyloid formation. FI was uniform at t =1.0 h ($2.0 \times 10^4 \pm 0.4 \times 10^4$) when amyloids had not yet formed (Figure 3B). F suddenly increased in some droplets, indicating amyloid formation, but it did not increase in others (Figure 3A and B). These results showed that amyloid formation was stochastic in the droplets, indicating the occurrence of amyloid nucleation. After F increased, the fibrils extended from the droplets (e.g., 5.5 h in Figure 3A), similar to a previous observation of amyloid formation in droplets *in vitro*[8].

To distinguish between droplets with and without amyloid nucleation, the threshold of F ($F_{\text{threshold}}$) was determined as 4×10^4 (Equation S2 in Supporting Information). A total of 300 droplets, with diameters ranging from 2.5 to 8.0 μm, were sorted by size and equipartitioned into four size ranges. The ratio of the number of droplets with nucleation to the total number of

droplets ($N_{\text{nucleation}}/N_{\text{total}}$) was calculated for each size range. $N_{\text{nucleation}}/N_{\text{total}}$ increased with time and size (Figure 3C). Because the nuclei in a droplet did not exhibit a transfer to other droplets (Figure 2D), the nucleation event in each droplet was independent. Therefore, $N_{\text{nucleation}}/N_{\text{total}}$ reflects the probability that nucleation events occur inside a droplet of volume V during time τ (Equation S3 and S4 in Supporting Information). The time evolution of $N_{\text{nucleation}}/N_{\text{total}}$ was analyzed using the two-step nucleation model, which is a common model to describe amyloid nucleation (Figure 3D)[23,25,35–38].This model assumes that the oligomers of amyloidogenic protein formed reversibly from monomers, becoming nuclei in the amyloid. When the first nucleation event in the droplet can induce a sufficiently high increase in F to exceed $F_{\text{threshold}}$, $N_{\text{nucleation}}/N_{\text{total}}$ is described as follows by combining the rate equations of the two-step nucleation model with Poisson distribution:

$$\frac{N_{\text{nucleation}}}{N_{\text{total}}} = 1 - exp\left(-\frac{Vk_o k_{conv} {C_{droplet}}^{n_o+n_{conv}} t^2}{2}\right)$$
$$= 1 - exp\left(-\frac{VJt}{2}\right) \quad (1)$$

where k_o is the rate constant of oligomer formation from monomers; k_f is the rate constant of oligomer conversion into fibrils (or nuclei); C_{droplet} is the Sup35NM monomer concentration in droplets; n_o is the reaction order of oligomer formation from monomers; and n_{conv} is the reaction order of oligomer conversion into fibrils (Supporting Information). The time change in $N_{\text{nucleation}}/N_{\text{total}}$ was reproduced by Equation 1 (Figure 3C) and the time constant ($JV/2t$, Figure 3E) increased with droplet size. By dividing $JV/2t$ by the droplet volume (V) of each size range, the nucleation rate $J/t = k_o k_f {C_{droplet}}^{n_o+n_{conv}}$ $\text{m}^{-3}\text{s}^{-2}$ (Equation S5 and Supporting Information) was calculated as approximately 10^7 m^{-3} s^{-1} and was insensitive to the droplet size (Figure 3F). The analytical results with a different number of size ranges are reported in Figure S3 The reproducibility is shown in Figure S4. The addition of agarose and PEG did not affect the nucleation rate (Figure S5).

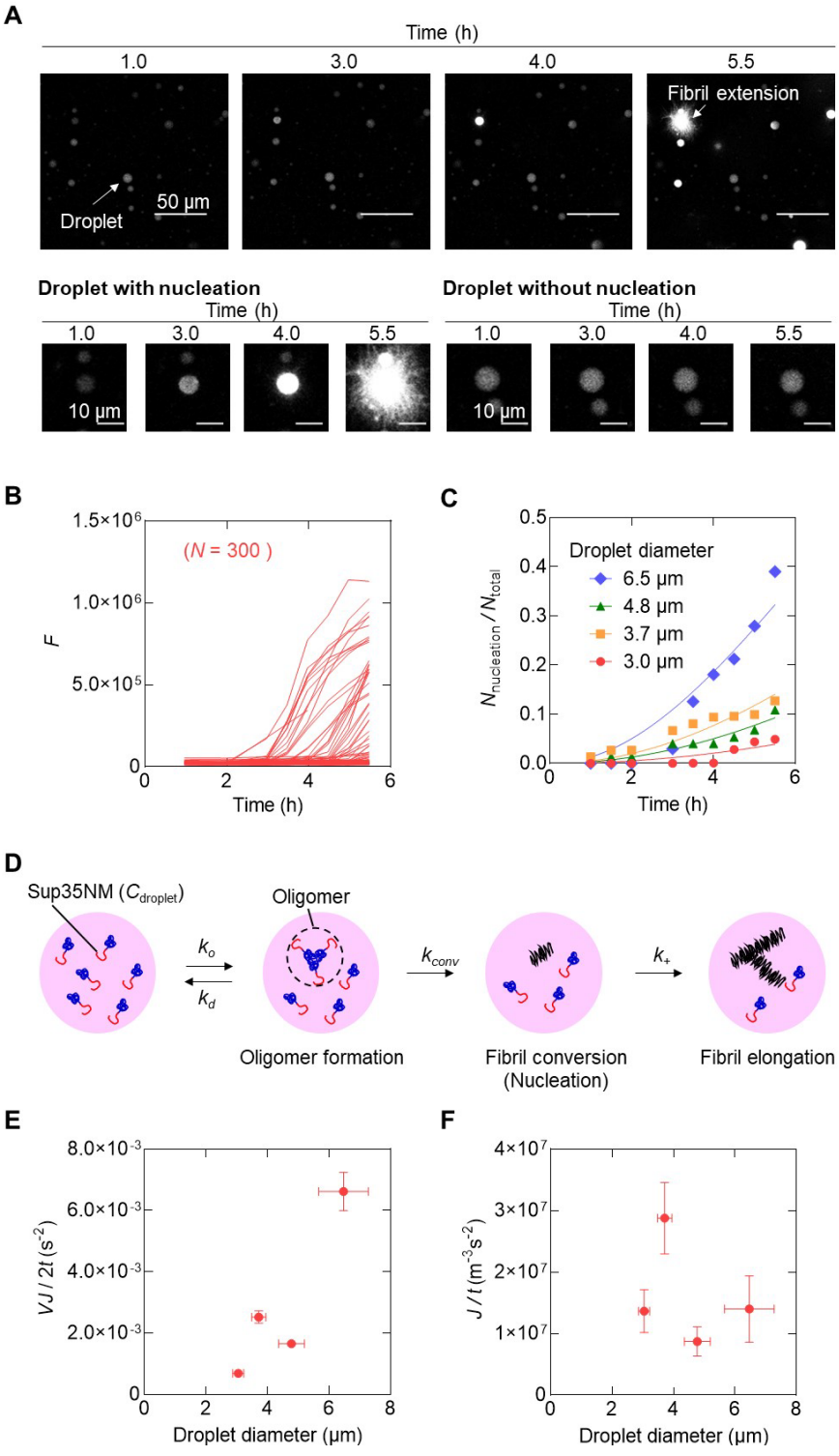

Figure 3. Amyloid formation in Sup35NM droplets. (A) Confocal micrographs of Sup35NM droplets showing fluorescence from ThT. Fluorescence intensity increased with time owing to amyloid formation. The lower row of micrographs depict examples of droplets with and without nucleation. (B) Time evolution of normalized fluorescence intensity (F) of the droplets. (C) Time evolution of the ratio of droplets in which more than one nucleus was generated ($N_{\mathrm{nucleation}}/N_{\mathrm{total}}$). The curve indicates the fitting based on Equation S6. (D) Schematic illustration of two-step nucleation in a Sup35NM droplet. In the droplet (pink

circle), Sup35NM oligomers gradually form. Oligomers are converted into fibrils at a rate constant of k_{conv}. Amyloid fibrils grow at an elongation rate constant of k_+. (E) Time constant of Equation S7 ($VJ/2t$) versus droplet diameter. The error bars on the X-axis indicate the standard deviations of the droplets. The error bars on the Y-axis reflect standard deviations of the fitting in Figure 3C. (F) Nucleation rate (J/t) versus droplet diameter. The error bars on the X-axis indicate the standard deviations of the droplets. The error bars on the Y-axis reflect the propagations of standard deviations of VJ/t and the droplet volume, V.

To discuss the effect of LLPS on amyloid nucleation, Sup35NM amyloid nucleation in the droplets was compared with that in an aqueous solution. Here, the ThT FIs of Sup35NM aqueous solutions and droplet suspension were measured in a 384-well plate, using a plate reader. The aqueous solution contained the same matrix as that in the droplet experiment, except PEG. As shown in Figure 4A, the time evolution of ThT FI was faster with the droplets than without them, even when the total Sup35NM amount in the well was the same (FI before normalization is shown in Figure S6A). The inverse of the lag time ($1/t_{lag}$) of the ThT FI, which is often used for the semi-quantitative comparison of the amyloid nucleation rate[7,39], was higher with droplets than in solutions (Figure 4B). From these results, it was conventionally interpreted that droplet formation enhanced amyloid nucleation. However, the comparison of the kinetic parameters of amyloid nucleation (J/t and J_{mol}/t in Figure 4C and D) between the droplets and aqueous solutions showed the opposite tendency: droplet formation suppressed amyloid nucleation. FI was analyzed using the global fit of the secondary nucleation model in Amylofit[40] rate constants in the secondary nucleation model into those in the two-step nucleation model (explained in Section 3, Supporting Information). The rate constants in the solutions were determined as $k_o k_{conv} = (10 \pm 8) \times 10^{-6}\ M^{1-n_o-n_{conv}}\ s^{-2}$ and $n_o + n_{conv} = 3.0$ (Figure 4C, Table S1) by assuming fibril elongation rate constant (k_+) as $2\times 10^5\ M^{-1}s^{-1}$(Supporting information section 3)[41]. Next, we calculated the nucleation rate per mol ($J_{mol} = J/tC = k_o k_{conv} C^{n_o+n_{conv}-1}$ (mol $^{-1}$ s^{-2})), instead of per volume. J_{mol} is essential to compare the risk of amyloid nucleation before and after LLPS because the molecular amount of amyloidogenic protein (AP) in a cell is preserved (Figure 1A). In experiments using an aqueous solution, J_{mol} increased with an increase in Sup35NM concentration because $n_o+n_{conv} - 1 = 2.0$. Surprisingly, J_{mol} was lower in the droplets than in the aqueous solution when Sup35NM concentration in solution (C_{sol}) $\geq C^* \approx 10$ μM. This means that the nucleation was slower in the droplets than in the solution if $C_{sol} \geq C^*$. It should be noted that this tendency can be reproduced by kinetic analysis using Amylofit under several assumptions (Figure S6B and C, and Table S2). The observation of J_{mol} opposes the conclusion from the comparison of t_{lag} (Figure 4B) and the previous simulation work predicting that droplet nucleation would accelerate at higher concentration ranges owing to increasing oligomer size[22,24,25]. Our findings highlight that LLPS reduces the risk of amyloid formation of Sup35NM when C_{sol} is higher than $C^* \approx 10$ μM.

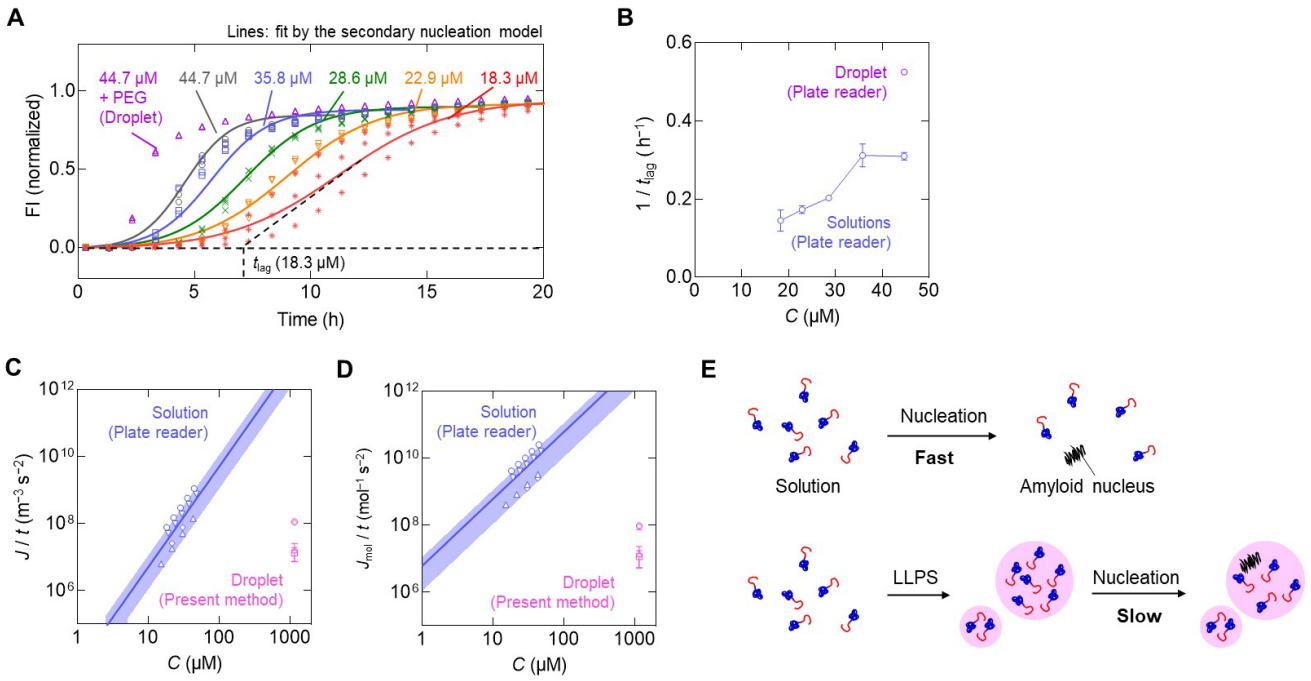

Figure 4. Comparison of amyloid nucleation rates between droplets and solutions. (A) Time evolution of ThT fluorescence intensity (FI) measured using a plate reader ($N = 3$). (B) Comparison of the inverse of lag time ($1/t_{lag}$). The error bars indicate the standard deviation (SD) of three experiments. (C) Comparison of the amyloid nucleation rate (J/t) in solution measured by a plate reader and droplets measured via the proposed method. The different symbols indicate different series of experiments conducted on different days. The pale blue area and error reflect the standard deviations of J/t. (D) Comparison of the amyloid nucleation rate per mol (J_{mol}/t) in solution measured by a plate reader and droplets measured via the proposed method. The pale blue area and error bars reflect the propagations of the SDs of J/t. The error bars reflect the standard deviations of J_{mol}/t. Higher $1/t_{lag}$, J/t, and J_{mol}/t values indicate faster amyloid nucleation. (E) Schematic of nucleation rates in solution and in Sup35NM droplets.

Discussion

In this study, we quantified amyloid nucleation rates in droplets of AP using a developed image analytical method. The results revealed that the nucleation rates in Sup35NM droplets were lower than those in aqueous solutions when $C_{sol} > C^*$ (10 μM). In LLPS conditions achieved using PEG, the binodal concentration ($C_{binodal}$), which is the same as the concentration of protein-depleted phase C', was 18 μM. Since $C_{binodal} > C^*$, LLPS did not enhance amyloid nucleation but suppressed it (Figure 4E). It should be noted that the relationship between C^* and $C_{binodal}$ changed depending on the protein species and LLPS conditions, such as PEG concentrations, pH, and additives. We found that droplet formation condensed the proteins and could suppress amyloid formation at high protein concentrations, suggesting that droplet formation suppresses unwilling protein aggregation, despite hypotheses predicting the opposite[7,8,22,24]. In contrast to *in vitro*/*in silico* investigations of amyloid nucleation in droplets, the LLPS-mediated enhancement of amyloid formation has seldom been observed *in vivo*. To our knowledge, amyloid formation enhancement via LLPS *in vivo* has only been confirmed for α-synuclein to date[7]. We believe

that our findings will bridge the gap between *in vivo* and *in vitro* observations and provide novel insights into the role of LLPS in amyloidosis-related proteins from a pathological perspective.

Moreover, our findings indicated that the comparison of the lag time (t_{lag})[7,39] with the time evolution of ThT FI, which is conventionally used to evaluate the amyloid nucleation rate qualitatively, does not necessarily reflect the intrinsic amyloid nucleation rates. To compare the nucleation rate between droplets and solutions, a detailed reaction kinetic analysis, as performed in this study, is needed, even if the total amount of the AP is the same.

The present method indicated the rate reduction of $J/t = k_o k_{conv} C^{n_o + n_{conv}}$ in the droplets but could not indicate the rate reduction of oligomer formation from monomers ($k_o C^{no}$) and oligomer conversion into fibrils ($k_{conv} C^{n_{conv}}$) separately. Although the mechanism of suppression was not clear, we speculate that the physicochemical properties of the droplets may be involved. For instance, the high viscosity of the droplets[42] reduces the nucleation rate, as is thought to occur in semi-crystalline polymers[43]. Specifically, the diffusion coefficient of Sup35NM in the droplets, as measured using FRAP, was 10^{-15} m^2/s, which is much lower than that in the aqueous solution (10^{-10} m^2/s)[29]. The stabilization of certain protein structures in the crowding environment[44] of the droplets may reduce amyloid nucleation. The detailed molecular mechanism must be investigated using other analytical methods, such as fluorescence protein–protein interaction analysis. Future investigations on the relationship between droplet size and nucleation will deepen our understanding of amyloid nucleation from droplets.

Conclusion

In this study, we examined the kinetics of amyloid nucleation in droplets of Sup35NM. The nucleation was suppressed by LLPS above the critical concentration (C^*) and enhanced below C^*. In addition, results from the ThT assay, a wide-spread semi-quantitative method for measurement of the amyloid nucleation rate, did not necessarily reflect the amyloid nucleation rate in droplets and can potentially overestimate it. We expect that these findings will not only aid in bridging the gap between the nucleation behavior in aqueous solution and condensed matters but also provide new insights into the role of LLPS in amyloidosis-related proteins from a pathological perspective.

Conflicts of interest

There are no conflicts to declare.

Supporting Information

Electronic Supplementary Information (ESI) available: Experiment details, materials, and methods, and supplemental figures/tables, including bright field and confocal micrographs of ThT fluorescence, time course of Sup35NM droplet size, estimation of droplet nucleation number, Order estimation of $k_d + k_{conv} C^{n_{conv}}$, droplet *J/t* differences, reproducibility of amyloid nucleation from Sup35NM droplets, Effect of PEG and agarose concentrations on amyloid nucleation rate, Amyloid formation, images of non-nucleated and nucleated droplets, kinetic parameters of Sup35NM amyloid formation, and summary of nucleated and non-nucleated droplet numbers (DOC)

Author Contribution

M.F. conceived and designed the research; M.F., N.S., Y.O., E.C., and K.S. designed the experiments; S.N., Y.O., and K.S. prepared proteins; M.F., Y.M., and T.O. acquired and analyzed the experimental data; S.T., M.K., M.G., and A.H. advised the research. The manuscript was prepared by M.F. All authors have given approval to the final version of the manuscript.

ACKNOWLEDGEMENT

This work was supported by Japan Society for the promotion of Science (Grant-in-Aid for Scientific Research on Innovative Areas, 20H04691, and Grant-in-Aid for Challenging Research (Exploratory),22K19284), Japan Science and Technology Agency (FOREST, JPMJFR211Y) , Naito Science & Engineering Foundation and MEXT Program for Supporting Construction of Core Facilities (JPMXS0440600021 and JPMXS0440600022). The authors would like to express sincere gratitude to Prof. Kazumasa Ohashi, Ms. Eiko Hanzawa, Prof. Eriko Nango, and Prof. Takaaki Fujiwara of the Tohoku University for their technical support.

REFERENCES

[1] M. R. Sawaya, M. P. Hughes, J. A. Rodriguez, R. Riek, D. S. Eisenberg, The expanding amyloid family: Structure, stability, function, and pathogenesis. *Cell* **2021**, *184*, 4857–4873.

[2] T. P. J. Knowles, M. Vendruscolo, C. M. Dobson, the amyloid state and its association with protein misfolding diseases.. *Nat. Rev. Mol. Cell Biol.* **2014**, *15*, 384–396.

[3] R. Crespo, F. A. Rocha, A. M. Damas, P. M. Martins, A generic crystallization-like model that describes the kinetics of amyloid fibril formation. *J. Biol. Chem.* **2012**, *287*, 30585–30594.

[4] J. T. Jarrett, P. T. Lansbury, Seeding “one-dimensional crystallization” of amyloid: A pathogenic mechanism in Alzheimer’s disease and scrapie?*Cell* **1993**, *73*, 1055–1058.

[5] T. P. J. Knowles, C. A. Waudby, G. L. Devlin, S. I. A. Cohen, A. Aguzzi, M. Vendruscolo, E. M. Terentjev, M. E. Welland, C. M. Dobson, An analytical solution to the kinetics of breakable filament assembly. *Science* **2009**, *326*, 1533–1537.

[6] Y. Yoshimura, Y. Lin, H. Yagi, Y. H. Lee, H. Kitayama, K. Sakurai, M. So, H. Ogi, H. Naiki, Y. Goto, Distinguishing crystal-like amyloid fibrils and glass-like amorphous aggregates from their kinetics of formation. *Proc. Natl. Acad. Sci. U. S. A.* **2012**, *109*, 14446–14451.

[7] S. Ray, N. Singh, R. Kumar, K. Patel, S. Pandey, D. Datta, J. Mahato, R. Panigrahi, A. Navalkar, S. Mehra, L. Gadhe, D. Chatterjee, A. S. Sawner, S. Maiti, S. Bhatia, J. A. Gerez, A. Chowdhury, A. Kumar, R. Padinhateeri, R. Riek, G. Krishnamoorthy, S. K. Maji, α -synuclein aggregation nucleates through liquid–liquid phase separation. *Nat. Chem.* **2020**, *12*, 705–716.

[8] A. Patel, H. O. Lee, L. Jawerth, S. Maharana, M. Jahnel, M. Y. Hein, S. Stoynov, J. Mahamid, S. Saha, T. M. Franzmann, A. Pozniakovski, I. Poser, N. Maghelli, L. A. Royer, M. Weigert, E. W. Myers, S. Grill, D. Drechsel, A. A. Hyman, S. Alberti, A liquid-to-solid phase transition of the ALS protein FUS accelerated by disease mutation. *Cell* **2015**, *162*, 1066–

1077.

[9] S. Ambadipudi, J. Biernat, D. Riedel, E. Mandelkow, M. Zweckstetter, *Nat. Commun.* Liquid-liquid phase separation of the microtubule-binding repeats of the Alzheimer-related protein Tau. **2017**, *8*, 1–13.

[10] N. M. Kanaan, C. Hamel, T. Grabinski, B. Combs, Liquid–liquid phase separation induces pathogenic tau conformations in vitro. *Nat. Commun.* **2020**, *11*, 1–16.

[11] W. M. Babinchak, R. Haider, B. K. Dumm, P. Sarkar, K. Surewicz, J. K. Choi, W. K. Surewicz, The role of liquid–liquid phase separation in aggregation of the TDP-43 low-complexity domain. *J. Biol. Chem.* **2019**, *294*, 6306–6317.

[12] N. Sekiyama, K. Takaba, S. Maki-Yonekura, K. I. Akagi, Y. Ohtani, K. Imamura, T. Terakawa, K. Yamashita, D. Inaoka, K. Yonekura, T. S. Kodama, H. Tochio, ALS mutations in the TIA-1 prion-like domain trigger highly condensed pathogenic structures. *Proc. Natl. Acad. Sci. U. S. A.* **2022**, *119*, e2122523119.

[13] A. Molliex, J. Temirov, J. Lee, M. Coughlin, A. P. Kanagaraj, H. J. Kim, T. Mittag, J. P. Taylor, Phase separation by low complexity domains promotes stress granule assembly and drives pathological fibrillization. *Cell* **2015**, *163*, 123–133.

[14] T. M. Franzmann, M. Jahnel, A. Pozniakovsky, J. Mahamid, A. S. Holehouse, E. Nüske, D. Richter, W. Baumeister, S. W. Grill, R. V. Pappu, A. A. Hyman, S. Alberti, Phase separation of a yeast prion protein promotes cellular fitness. *Science* **2018**, *359*, DOI 10.1126/SCIENCE.AAO5654/SUPPL_FILE/AAO5654S8.MP4.

[15] S. F. Banani, H. O. Lee, A. A. Hyman, M. K. Rosen, Biomolecular condensates: Organizers of cellular biochemistry. *Nat. Rev. Mol. Cell Biol.* **2017**, DOI 10.1038/nrm.2017.7.

[16] S. Boeynaems, S. Alberti, N. L. Fawzi, T. Mittag, M. Polymenidou, F. Rousseau, J. Schymkowitz, J. Shorter, B. Wolozin, L. van den Bosch, P. Tompa, M. Fuxreiter, Protein phase separation: A new phase in cell biology. *Trends Cell Biol.* **2018**, *28*, 420–435.

[17] W. M. Babinchak, W. K. Surewicz, Liquid–liquid phase separation and its mechanistic role in pathological protein aggregation. *J. Mol. Biol.* **2020**, *432*, 1910–1925.

[18] N. A. Yewdall, A. A. M. André, T. Lu, E. Spruijt, Coacervates as models of membraneless organelles. *Curr. Opin. Colloid Interface Sci.* **2021**, *52*, 101416.

[19] C. Yuan, A. Levin, W. Chen, R. Xing, Q. Zou, T. W. Herling, P. K. Challa, T. P. J. Knowles, X. Yan, Nucleation and growth of amino acid and peptide supramolecular polymers through liquid–liquid phase separation. *Angew. Chem.* **2019**, *131*, 18284–18291.

[20] W. Mori, R. Kawakami, Y. Niko, T. Haruta, T. Imamura, K. Shiraki, T. Zako, Differences in interaction lead to the formation of different types of insulin amyloid. *Sci. Rep.* **2022**, *12*, 1–15.

[21] L. Guo, H. J. Kim, H. Wang, J. Monaghan, F. Freyermuth, J. C. Sung, K. O'Donovan, C. M. Fare, Z. Diaz, N. Singh, Z. C. Zhang, M. Coughlin, E. A. Sweeny, M. E. DeSantis, M. E. Jackrel, C. B. Rodell, J. A. Burdick, O. D. King, A. D. Gitler, C. Lagier-Tourenne, U. B. Pandey, Y. M. Chook, J. P. Taylor, J. Shorter, Nuclear-import receptors reverse aberrant phase transitions of RNA-binding proteins with prion-like domains. *Cell* **2018**, *173*, 677-692.e20.

[22] Y. Xing, A. Nandakumar, A. Kakinen, Y. Sun, T. P. Davis, C. Ke, F. Ding, Amyloid aggregation under the lens of liquid−liquid phase separation. *J. Phys. Chem. Lett.* **2020**, *12*, 378.

[23] D. Kashchiev, R. Cabriolu, S. Auer, Confounding the paradigm: Peculiarities of amyloid fibril nucleation. *J. Am. Chem. Soc.* **2013**, *135*, 1531–1539.

[24] A. Šarić, Y. C. Chebaro, T. P. J. Knowles, D. Frenkel, Crucial role of nonspecific interactions in amyloid nucleation. *Proc. Natl. Acad. Sci. U. S. A.* **2014**, *111*, 17869–17874.

[25] T. C. T. Michaels, A. Šarić, S. Curk, K. Bernfur, P. Arosio, G. Meisl, A. J. Dear, S. I. A. Cohen, C. M. Dobson, M. Vendruscolo, S. Linse, T. P. J. Knowles, Dynamics of oligomer populations formed during the aggregation of Alzheimer's Aβ42 peptide*Nat. Chem.* **2020**, *12*, 445–451.

[26] Y. Shin, C. P. Brangwynne, Liquid phase condensation in cell physiology and disease. *Science* **2017**, 357, 6357.

[27] B. Y. Feng, B. H. Toyama, H. Wille, D. W. Colby, S. R. Collins, B. C. H. May, S. B. Prusiner, J. Weissman, B. K. Shoichet, mall-molecule aggregates inhibit amyloid polymerization. *Nat. Chem. Biol.* **2008**, *4*, 197–199.

[28] R. Krishnan, S. L. Lindquist, Structural insights into a yeast prion illuminate nucleation and strain diversity. *Nature* **2005**, *435*, 765–772.

[29] Y. Ohhashi, Y. Yamaguchi, H. Kurahashi, Y. O. Kamatari, S. Sugiyama, B. Uluca, T. Piechatzek, Y. Komi, T. Shida, H. Müller, S. Hanashima, H. Heise, K. Kuwata, M. Tanaka, Molecular basis for diversification of yeast prion strain conformation. *Proc. Natl. Acad. Sci. U. S. A.* **2018**, *115*, 2389–2394.

[30] P. M. Tessier, S. Lindquist, Prion recognition elements govern nucleation, strain specificity and species barriers. *Nature* **2007**, 447, 556–561.

[31] Y. O. Chernoff, A. V. Grizel, A. A. Rubel, A. A. Zelinsky, P. Chandramowlishwaran, T. A. Chernova, Application of yeast to studying amyloid and prion diseases. *Adv. Genet.* **2020**, *105*, 293–380.

[32] M. Linsenmeier, M. R. G. Kopp, F. Grigolato, L. Emmanoulidis, D. Liu, D. Zürcher, M. Hondele, K. Weis, U. Capasso Palmiero, P. Arosio, *Angew. Chem.* **2019**, Dynamics of synthetic membraneless organelles in microfluidic droplets. *131*, 14631–14636.

[33] J. R. Glover, A. S. Kowal, E. C. Schirmer, M. M. Patino, J. J. Liu, S. Lindquist, elf-seeded fibers formed by Sup35, the protein determinant of [PSI+], a heritable prion-like factor of S. cerevisiae. *Cell* **1997**, *89*, 811–819.

[34] M. Mimura, S. Tomita, Y. Shinkai, T. Hosokai, H. Kumeta, T. Saio, K. Shiraki, R. Kurita, Quadruplex folding promotes the condensation of linker histones and DNAs via liquid–liquid phase separation. *J. Am. Chem. Soc.* **2021**, *143*, 9849–9857.

[35] A. J. Dear, T. C. T. Michaels, G. Meisl, D. Klenerman, S. Wu, S. Perrett, S. Linse, C. M. Dobson, T. P. J. Knowles, Kinetic diversity of amyloid oligomers. *Proc. Natl. Acad. Sci. U. S. A.* **2020**, *117*, 12087–12094.

[36] D. Kashchiev, P. G. Vekilov, A. B. Kolomeisky, Kinetics of two-step nucleation of crystals. *J. Chem. Phys.* **2005**, *122*,

244706.

[37] D. Gebauer, M. Kellermeier, J. D. Gale, L. Bergström, H. Cölfen, Pre-nucleation clusters as solute precursors in crystallisation.*Chem. Soc. Rev.* **2014**, *43*, 2348–2371.

[38] E. Chatani, R. Inoue, H. Imamura, M. Sugiyama, M. Kato, M. Yamamoto, K. Nishida, T. Kanaya, Early aggregation preceding the nucleation of insulin amyloid fibrils as monitored by small angle X-ray scattering. *Sci. Rep.* **2015**, DOI 10.1038/srep15485.

[39] A. S. Sawner, S. Ray, P. Yadav, S. Mukherjee, R. Panigrahi, M. Poudyal, K. Patel, D. Ghosh, E. Kummerant, A. Kumar, R. Riek, S. K. Maji, Modulating α-synuclein liquid–liquid phase separation. *Biochemistry* **2021**, *60*, 3676–3696.

[40] G. Meisl, J. B. Kirkegaard, P. Arosio, T. C. T. Michaels, M. Vendruscolo, C. M. Dobson, S. Linse, T. P. J. Knowles, *Nat. Protoc.* Molecular mechanisms of protein aggregation from global fitting of kinetic models. **2016**, *11*, 252–272.

[41] H. Konno, T. Watanabe-Nakayama, T. Uchihashi, M. Okuda, L. Zhu, N. Kodera, Y. Kikuchi, T. Ando, H. Taguchi, High-speed atomic force microscopy reveals structural dynamics of amyloid β1-42 aggregates. *Proc Natl Acad Sci U S A* **2020**, 117 (14), 7831–7836.

[42] S. Elbaum-Garfinkle, Y. Kim, K. Szczepaniak, C. C. H. Chen, C. R. Eckmann, S. Myong, C. P. Brangwynne, The disordered P granule protein LAF-1 drives phase separation into droplets with tunable viscosity and dynamics. *Proc. Natl. Acad. Sci. U. S. A.* **2015**, *112*, 7189–7194.

[43] K. F. Kelton, A. L. Greer, Nucleation in Condensed Matter – Applications in Materials and Biology*, Elsevier,* 2010, *Volume 15*, 726.

[44] K. Nakajima, K. Yamaguchi, M. Noji, C. Aguirre, K. Ikenaka, H. Mochizuki, L. Zhou, H. Ogi, T. Ito, I. Narita, F. Gejyo, H. Naiki, S. Yamamoto, Y. Goto, Macromolecular crowding and supersaturation protect hemodialysis patients from the onset of dialysis-related amyloidosis. *Nat. Commun.* **2022**, *13*, 1–13.